An Atlas-based Whole-brain Fiber-tracking Method with Automatic Setting of an Optimal Starting Plane in all Parcels

Shiho Okuhata[*1], Hodaka Miki[1], Ryusuke Nakai[2], Tetsuo Kobayashi[1]

[1]*Graduate School of Engineering, Kyoto University, Kyoto, Japan;* [2]*Kokoro Research Center, Kyoto University, Kyoto, Japan*

Abstract:

Background*:* The fiber-tracking based on diffusion magnetic resonance imaging technique is one of the methods that indirectly examine the structural information about the cerebral white matter in vivo. Conventionally, fiber-tracking approaches are accompanied with manual settings of the starting regions of fiber tracking, which is usually very time-consuming and unsuitable for large-scale data analysis. ***Objective****:* In order to clarify the physical fiber connections associated with disease-specific neural circuits for various neuropsychiatric disorders, we proposed an automated diffusion magnetic resonance imaging based whole-brain fiber-tracking method combined with an atlas separating 54 regions of the white matter. ***Methods****:* The propose method automatically set the fiber-tracking starting plane in each parcel and rotated along the running direction of fibers as well so that it enabled swift, objective, and reproducible analysis. The method was verified with real diffusion magnetic resonance imaging data recorded from three healthy volunteers. ***Results****:* The mean fiber direction for each parcel was confirmed to fit the anatomical configuration. The fiber-tracking streamlines were confirmed to run along the first eigenvector of diffusion tensor and to terminate according to the pre-set termination condition. The major fiber tracts of the 54 white matter parcels were relevantly reconstructed. ***Conclusion****:* The results demonstrate the feasibility of the proposed automated whole-brain atlas-based fiber-tracking method for investigating white matter disruptions associated with neuropsychiatric disorders especially in large-scale datasets.

Keywords: Diffusion weighted magnetic resonance imaging; white matter atlas; tractography; automatic setting; whole-brain analysis; tensor deflection

1. INTRODUCTION

Diffusion magnetic resonance imaging (dMRI) is an important tool for both basic and neuropsychiatric clinical studies to measure the diffusion phenomenon of water molecules reflecting thermal Brownian motion using motion-probing gradients of multiple axes in at least six spatial directions. Most dMRI studies of neuropsychiatric disorders have reported abnormalities in the white matter integrity. In order to detect neural networks specific to neuropsychiatric disorders such as depression and schizophrenia, various approaches have been suggested and used.

Among these various approaches, voxel-based analysis is highly utilized because of its advantages of whole-brain, fully automated processes. However, one of its disadvantages is the high sensitivity to registration errors and possible false positives in the affected regions [1]. Region of interest (ROI)-based analysis limits the number of statistical testing by setting certain ROIs manually in order to avoid multiple comparisons. Setting the ROIs manually, however, can be potentially inaccurate, subjective, and time-consuming. Although ROI-based analysis is useful in local investigations of small sample sizes, it is not suitable for whole-brain, large-scale investigations.

As an effective breakthrough, Tract-Based Spatial Statistics (TBSS) [2] was introduced and is currently widely used. TBSS attempts to reduce the effect of mis-registration by projecting all fractional anisotropy (FA) voxels onto the nearest position on a “skeleton” approximating the white matter tract [2]. Despite this advantage, the most problematic limitation, especially in the field of neuropsychiatric research, is that TBSS is highly correlated to the FA value, but the anatomical alignment is less accurate [3]. This is because each voxel is projected to the nearest skeleton location regardless of its anatomical attribution. In addition, white matter hyper-intensity and FA-reducing abnormalities are often observed in neuropsychiatric patients, and pose serious problems because these conditions violate the assumption of TBSS that local FA maxima are anatomically located in white matter tract centers [4].

Fiber-tracking is a method that indirectly examines structural information about the cerebral white matter in vivo. By quantifying the magnitude and direction of water diffusion, fiber-tracking accurately identifies white matter fascicles in the living human brain [5,6]. Although the reconstructed pathways do not necessarily correspond to the anatomical white

*Dr. Shiho Okuhata, Graduate School of Engineering, Kyoto University, 615-8510, Kyoto-daigaku katsura, Nishikyo-ku, Kyoto-shi, Kyoto, Japan; Tel/Fax: +81-75-383-2259; E-mails: sokuhata@kuee.kyoto-u.ac.jp

matter bundles [7], evidence from postmortem studies has demonstrated significant correspondence between diffusion weighted-derived pathways and anatomical data [8]. In the fiber tracking based analysis, fiber connection information (i.e., whether or not the voxels are estimated to be connected as a reconstructed fiber) based on the principal diffusion direction is particularly meaningful and only those with connection information are further evaluated. Unlike the voxel-based method and TBSS, most fiber-tracking methods require the manual setting of the starting ROIs and clustering of the reconstructed fiber tract, which is susceptible to subjectivity in many cases.

Though it is true that these various dMRI analysis approaches have accumulated evidence, white matter regions that are altered in schizophrenia or depression are widely diverse [i.e., 9-11]. As potential reasons for such inconsistencies, Kanaan et al. [12] pointed out to the small sample sizes and differences in methodologies. Drawing a coherent conclusion from these widely varying results from separate studies is very difficult and these inconsistencies may impede the progress in the detection of neuropsychiatric disease-specific and/or disease-common network. Although limited to voxel-based studies, meta-analysis of dMRI studies have attempted to address this issue by detecting consistent regions for each neuropsychiatric disorder as follows: left frontal and left temporal regions of the white matter in schizophrenia [13] and superior longitudinal fasciculus and fronto-occipital fasciculus in depression [14, 15].

However, the most straightforward approach would be the application of one single analysis method to a large-scale data set. Thus, the development of automated, objective, and analytical methods with minimal disadvantages is one of the major requirements in this field. A prospective dMRI analysis in the field of neuropsychiatry should consider the inclusion of the following properties: whole-brain, automatic, and translatability to anatomical information. In this study, a new automated quantitative evaluation method of all white matter fiber bundles using diffusion tensor fiber-tracking and conserving connection information, combined with a precise atlas of the whole brain was proposed.

As compared to voxel-based analysis and TBSS, the proposed method led to the grouping of voxels within segmented, anatomically translatable tract systems based on fiber tracking. Thus, this method firstly prevented false positives caused by the tremendous number of multiple comparisons, while retaining the advantage of whole-brain approach. Secondly, in this method, diffusion information such as FA and MD (mean diffusivity) sampled from the points on the reconstructed fiber will be the target of further evaluation. In contrast, average diffusion information based on all the voxels within the region may include that of untargeted structures (by co-registration error). The problem becomes more apparent in parcels which include crossing fiber region. All-voxel-average in a parcel may include diffusion information from crossing fibers, thus may hamper precise evaluation of the targeted fiber group.

In addition, considering application to large data sets, the most unique feature of the proposed method was the implementation of automatic settings of an optimal starting plane for fiber-tracking for each parcel with varying morphologies. This optimal automatic starting plane setting included an automatic plane rotation to match the dominant direction of the fiber in attempts to track the fiber at the maximum length.

2. MATERIALS AND METHOD

2.1. dMRI acquisition

dMRIs were obtained from three healthy volunteers (all male, age 24.33 ± 0.58), using a Siemens Verio 3.0T scanner (Siemens Erlangen, Germany) at Kokoro Research Center, Kyoto University, Kyoto, Japan. The study protocol was approved by the ethics committee of the Graduate School of Engineering, Kyoto University (approval no. 201607).

The imaging conditions were as follows: Repetition time of 6,630 ms, echo time of 83.4 ms, 242-mm field of view, voxel size of 2.0 × 2.0 × 3.0 mm^3, image matrix of 216 × 216, 48 slices, 30 non-collinear directions of motion probing gradient (MPG), and b value of 1,000 s/mm^2. An image was also obtained with b = 0 s/mm^2.

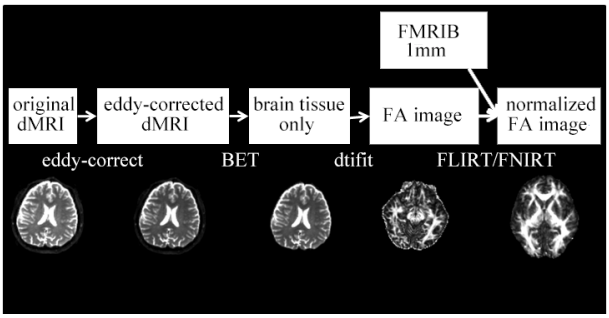

Fig. 1. *Flowchart of pre-processing.*

2.2. Pre-processing

Pre-processing (Fig. 1) was performed using the Functional MRI of the Brain (FMRIB) Software Library [16]. First, non-brain tissue was deleted with the brain extraction tool from an eddy current-corrected, diffusion-weighted image of the whole head. Second, the FMRIB Diffusion Toolbox was used to calculate diffusion indices such as FA, mean diffusivity (MD), tensor, and first eigenvectors. Finally, linear (affine) and non-linear registrations were performed using the FMRIB Linear Image Registration Tool followed by the FMRIB Nonlinear Image Registration Tool to normalize each diffusion image to a standard brain space.

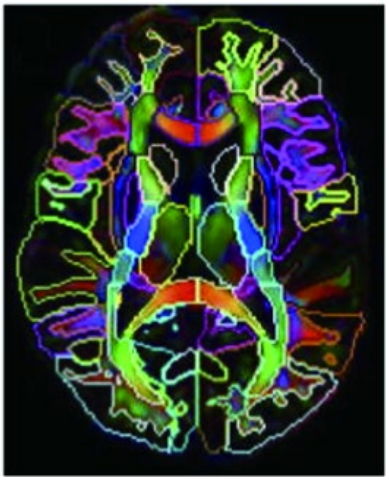

Fig. 2. *Johns Hopkins University (JHU) white matter atlas*

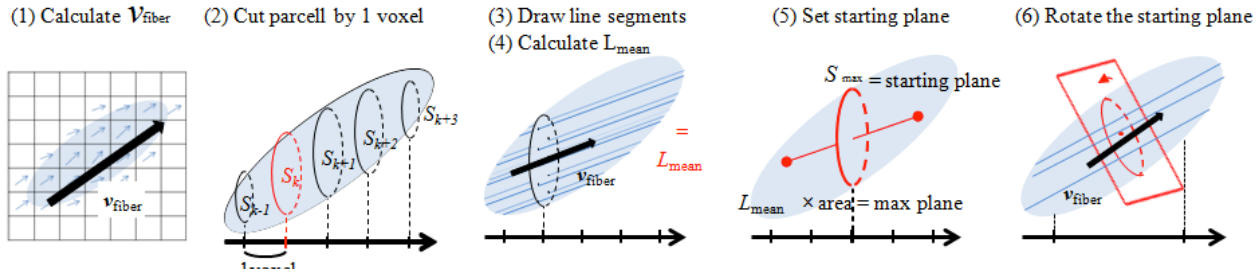

Fig. 3. *Schematic illustrations of the starting plane settings for fiber-tracking. (1) Calculate the dominant fiber orientation vector v_{fiber} in each parcel, (2) cut each parcel at multiple cross-sections with at an interval of one voxel, (3) draw line segments parallel to the dominant fiber orientation (v_{fiber}) inside the parcel at an interval of 0.25 mm, (4) calculate the mean length of all lines (L_{mean}), (5) create a cross-section with the maximum value of (L_{mean}) multiplied by its area as the starting plane, and (6) rotate the starting plane perpendicular to (v_{fiber}) (see also Fig. 4).*

2.3. Automated fiber-tracking method

We developed a fiber-tracking program using MATLAB for Windows (ver. 7.6.0.324; The MathWorks, Inc., Natick, MA, USA) for automated fiber-tracking, which included setting and rotating of the starting plane in each parcel.

2.3.1. Atlas for fiber-tracking

Johns Hopkins University Diffusion Tensor Imaging (JHU DTI)-based white-matter atlas was used as a template of fiber-tracking. In this atlas, the grey and white matters were separated into parcels according to the anatomical disposition (Fig. 2; JHU MNI SS WMPM Type II in MRI Studio [17-19]). In this study, 54 out of 159 white matter parcels were used for further fiber-tracking algorithms. Table 1 summarizes the list of all parcels and their abbreviations.

2.3.2. Automated setting and rotating of the starting plane of fiber-tracking

The starting plane of the fiber-tracking in each parcel was determined automatically according to the following steps (Fig. 3):

1. Calculate v_{fiber} in each parcel: A dominant fiber orientation vector in each parcel v_{fiber_each} was calculated by multiplying FA and e_1 over n voxels with FA > 0.25 as in equations (1) and (2). The FA threshold for the white matter was determined based on the fact that the grey matter typically has an FA of 0.05–0.15. An FA value of > 0.15–0.3 is commonly used as the FA threshold [20].

$$v_{fiber\_each} = \frac{1}{N}\sum_{k=1}^{N}(FA_k \times e_{1k}) \quad (1)$$

where e_{1k} is the first eigenvector at k-th voxel in each parcel and N is the total number of voxels in each parcel. Subsequently, mean v_{fiber_each} over all M subjects were calculated as follows:

$$v_{fiber} = \frac{1}{M}\sum_{k=1}^{M}(V_{fiber\_each_k}) \quad (2)$$

2. Cut each parcel at multiple cross-sections with the interval of 1 voxel.

3. Draw line-segments parallel to v_{fiber} inside the parcel with an interval of 0.25 mm.

4. Calculate the mean length of all lines (L_{mean}).

5. Set a cross-section having the maximum value of L_{mean} × its area as the starting plane.

6. Rotate the starting plane perpendicular to v_{fiber} (Fig. 4): After the centroid (x_{s0}, y_{s0}, z_{s0}) of the starting plane was determined, the starting plane was rotated perpendicular to V_{fiber} while keeping the center of gravity fixed. The starting point on the rotated starting plane (x_s, y_s, z_s) was obtained as follows:

$$\theta_x = \arccos\left(\frac{c}{\sqrt{b^2+c^2}}\right) \quad (3)$$

$$\theta_y = \arccos\left(\frac{a}{\sqrt{a^2+c^2}}\right) \quad (4)$$

$$\theta_z = \arccos\left(\frac{b}{\sqrt{a^2+b^2}}\right) \quad (5)$$

$$\begin{vmatrix} y_s \end{vmatrix} = \begin{vmatrix} 0 & \cos\theta_x & -\sin\theta_x \end{vmatrix} \begin{vmatrix} 0 & 1 & 0 \\ \sin\theta_z & \cos\theta_z & 0 \end{vmatrix} \begin{vmatrix} y_s - y_{s0} \end{vmatrix} + \begin{vmatrix} y_{s0} \end{vmatrix} \quad (6)$$

Where a, b, and c are the x, y, and z components of v_{fiber}.

2.3.3. Fiber-tracking

Fiber-tracking from the starting plane was performed using the tenor deflection method [21]. The interpolation was performed during the Runge-Kutta of the fourth order [22]. The stepping width was set at 0.5 mm. The starting points were dispersed evenly on the plane of the starting region at a rate of 4 points per mm^2; i.e., each starting point had a cross-sectional area of 0.25 mm^2.

Fiber-tracking was terminated at the parcel borders. In addition, it was terminated at a point with an FA < 0.25 within the parcel because FA decreases where the nerve fibers are not aligned and the tracking was considered to move away from the targeted nerve bundles. The FA value at the present step point was calculated via interpolation using the volume data for the center points of the nearest eight voxels around the step point. The tracking was also terminated when the flip angle was > 45° in order to exclude a large angular shift because the targeted bundles had a relatively linear shape. To identify and

erase erroneously tracked streamlines, the extracted streamline with the shortest length was selected separately for each hemisphere and used as the baseline streamline length. Any streamlines with a length exceeding 110 % of the baseline streamline length were judged to have an erroneous tracking result and were thus eliminated from the streamline group.

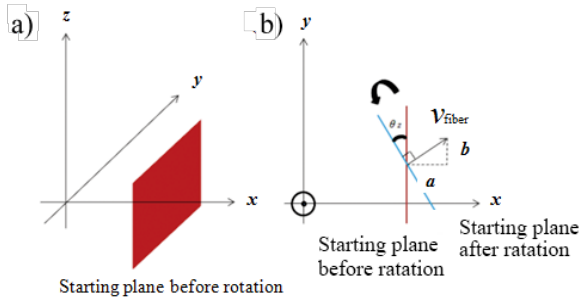

Fig. 4. *Schematic illustrations of starting plane rotation. a) The starting plane before automatic rotation. The starting plane was perpendicular to any of the three axes (x, y, or z). b) The starting plane after automatic rotation was perpendicular to the dominant fiber orientation vector.*

3. RESULTS

3.1. Fiber direction validation with a real dMRI

The automatic starting plane setting and tracking was firstly validated with the Cingulum (cingulate gyrus, CGC) parcel that slopes approximately 45° to the coordinate axis. Figure 5a depicts the tracking results of the CGC superimposed on the image of the first component of eigenvectors (green allows, x = 100) with an enlarged view (Fig. 5 b). The FA image of the CGC parcel is also superimposed. The tracked fibers are shown as blue lines with the automatically set and rotated reference surface. The streamlines of fiber-tracking were confirmed to run along the first eigenvector of diffusion tensor, and terminated in accordance with the termination condition (FA decrease and parcel border).

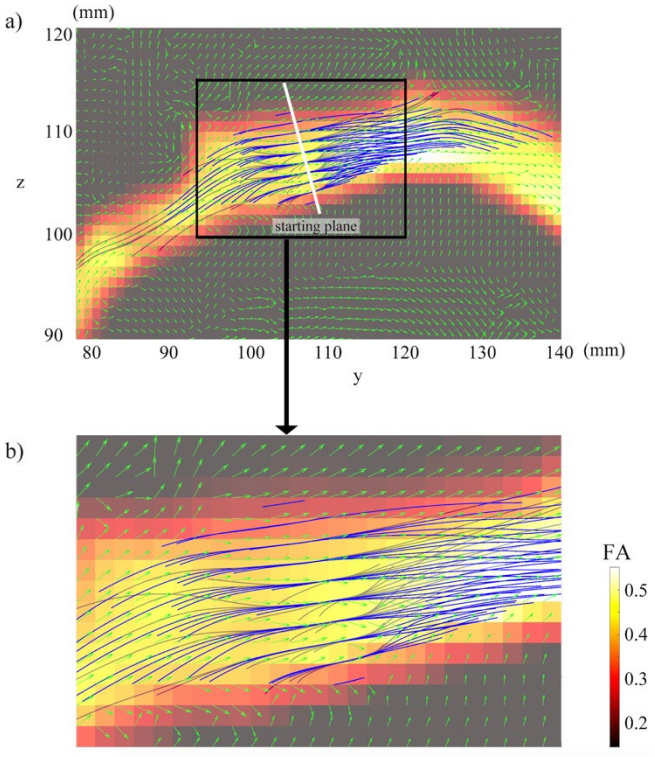

Fig. 5. *Tracking results of the cingulum (CGC) of x = 100. (a) The tracked fiber (blue lines) superimposed on the fractional anisotropy (FA) image and the first eigenvectors (green arrows) and (b) an enlarged view. Color plot of FA value is limited within CGC parcel for better visualization.*

Subsequently, whole brain automatic fiber tracking was carried out based on the mean vfiber_each (Fig. 6–9). Table 1 summarizes the direction of mean vfiber_each of all parcels calculated from three participants. Figure 6 shows the reconstructed corticospinal tracts (CST), superior cerebellar peduncle (SCP), cerebral peduncle (CP), and middle cerebellar peduncle (MCP) projected onto axial slices of z = -50 and -30. Red dots indicate the reconstructed fibers in the right hemisphere, and blue dots in the left hemisphere, projected onto the slices of the JHU atlas. Figure 7 shows the anterior limb of the internal capsule (ALIC), posterior limb of the internal capsule (PLIC), retrolenticular part of the internal capsule (RLIC), and external capsule (EC) projected onto axial slices of z = -10. Figure 8 shows the posterior thalamic radiation (PTR), anterior corona radiata (ACR), superior corona radiata (SCR), and posterior corona radiata (PCR) projected onto sagittal slices of x = 20 for the right hemisphere and x= -20 for the left hemisphere. CGC and cingulum (hippocampus, CGH) are depicted in Fig. 9 with the sagittal slice of x = 0.

4. DISCUSSION

The proposed method was validated using real dMRI obtained from three healthy controls. First, the result of a representative parcel (CGC) indicated that the fiber-tracking processes were completed with the configured settings and the streamlines of fiber-tracking were confirmed to run along the first eigenvector of diffusion tensor in each parcel. Second, the result of mean fiber direction, mean vfiber_each indicated that anatomically reasonable directions were automatically set for the major white matter parcels, and no discrepancy was shown in the same parcels of the contralateral hemisphere. For the minor parcels (i.e., fornix (cres)/stria terminalis [Fx/ST]), it may be necessary to calculate the mean vfiber_each from larger dataset to improve the reliability. In reality, we suggest retaining a database of mean vfiber_each and starting planes coordinates for all the parcels calculated from adequate numbers of dMRIs obtained from healthy volunteers, when apply it to newly acquired dataset.

Finally, the reconstructed fibers based on the proposed algorithm were in a good agreement with the anatomical fibers and shape of the JHU parcels. Although major fiber tracts such as CST reconstructed by the proposed method highly corresponded to the anatomical fiber tracts in shapes and directions, it is known that CST is anatomical extended far longer superiorly. Shortly terminated fiber tracking is one of the limitations of this method, and this is ascribed to the parcels specified by JHU white matter atlas. As the proposed algorithm limits the region for fiber-tracking within the target parcels (i.e., one of the termination condition of fiber-tracking), the

Table 1. *Parcel name lists of the John Hopkins University (JHU) white matter atlas and mean fiber direction calculated from real diffusion magnetic resonance diffusion imaging (dMRI) data.*

Parcel Name		Direction (right)	Direction (left)
CST	Corticospinal tract	I-S	I-S
ICP	Inferior cerebellar peduncle	I-S	I-S
ML	Medial lemniscus	I-S	I-S
SCP	Superior cerebellar peduncle	A-P	A-P
CP	Cerebral peduncle	I-S	I-S
ALIC	Anterior limb of internal capsule	A-P	A-P
PLIC	Posterior limb of internal capsule	I-S	I-S
PTR	Posterior thalamic radiation	A-P	A-P
ACR	Anterior corona radiata	A-P	A-P
SCR	Superior corona radiata	I-S	I-S
PCR	Posterior corona radiata	I-S	I-S
CGC	Cingulum (cingulate gyrus)	A-P	A-P
CGH	Cingulum (hippocampus)	I-S	I-S
Fx/ST	Fornix (cres)/stria terminalis	A-P	A-P
SLF	Superior longitudinal fasciculus	A-P	A-P
SFO	Superior fronto-occipital fasciculus	A-P	A-P
IFO	Inferior fronto-occipital fasciculus	A-P	A-P
SS	Sagittal stratum (include ILF and IFO)	A-P	A-P
EC	External capsule	I-S	I-S
UNC	Uncinate fasciculus	A-P	A-P
PCT	Pontine crossing tract (a part of mcp)	L-R	L-R
MCP	Middle cerebellar peduncle	I-S	I-S
Fx	Fornix (column and body of fornix)	I-S	I-S
GCC	Genu of corpus callosum	L-R	L-R
BCC	Body of corpus callosum	L-R	L-R
SCC	Splenium of corpus callosum	L-R	L-R
RLIC	Retrolenticular part of internal capsule	I-S	I-S

I: inferior, S: superior, A: anterior, P: posterior, L: left, and R: right.

reconstructed CST in the present study corresponds to a lower part of the anatomical CST. Similarly, the reconstructed uncinate fasciculus (UNC), inferior fronto-occipital fasciculus (IFO), superior fronto-occipital fasciculus (SFO), and superior longitudinal fasciculus (SLF) based on the present algorithm did not completely match the anatomical shape of the fiber tract, but were only part of these, which corresponded to the parcel shapes of JHU atlas. This limitation can be overcome by inter-connecting multiple adjacent parcels to broaden fiber-tracking target regions.

In addition, implementation of probabilistic [23] and global tracking [24] may be one of the strong options to overcome this limitation. Current dMRI acquisition in the clinical

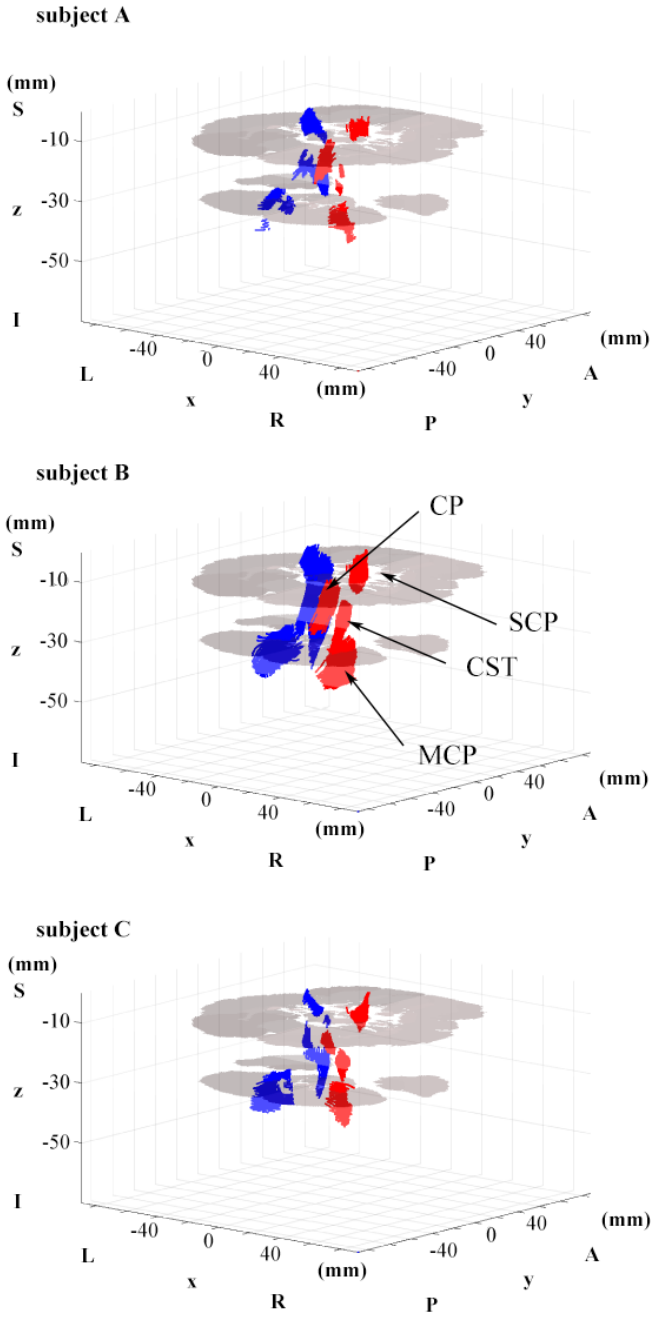

Fig. 6. *Tracked fibers in parcels corticospinal tracts (CST), superior cerebellar peduncle (SCP), cerebral peduncle (CP), and middle cerebellar peduncle (MCP) projected onto axial slices of John Hopkins University (JHU) atlas (z = -50, -30). Tracked fibers are shown in red dots (the right hemisphere) and blue dots (the left hemisphere).sphere) and blue dots (the left hemisphere).*

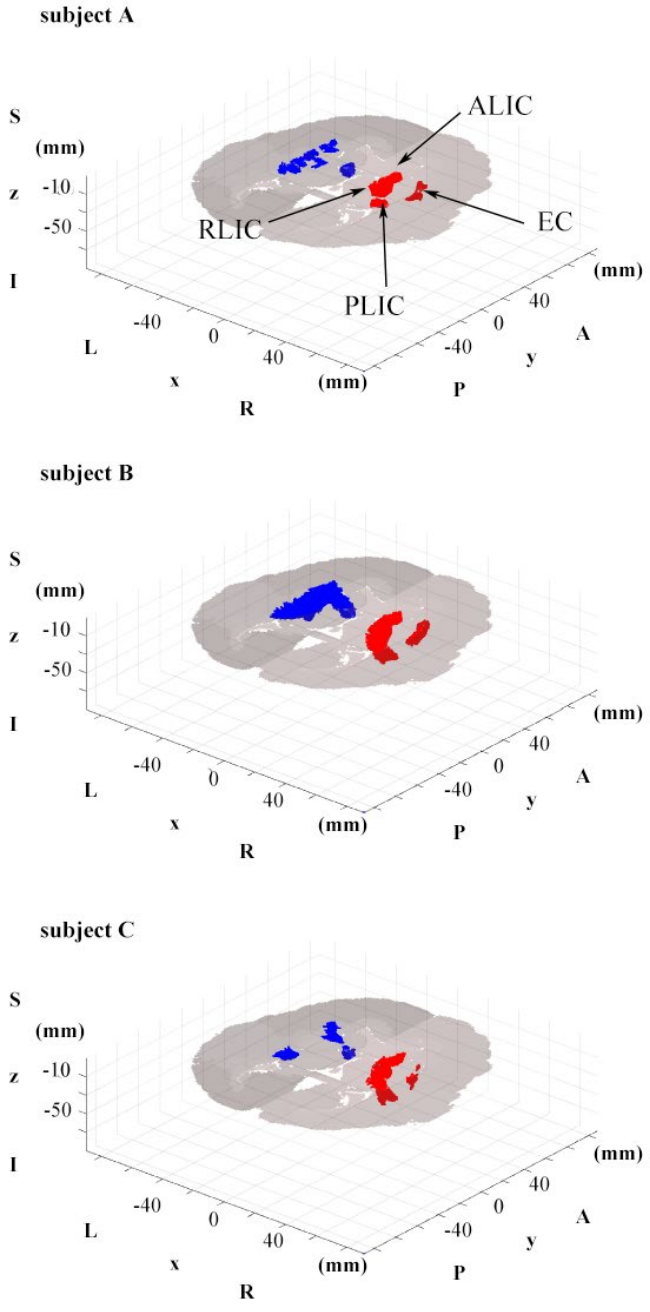

Fig. 7. *Tracked fibers in parcels anterior limb of the internal capsule (ALIC), posterior limb of the internal capsule (PLIC), retrolenticular part of the internal capsule (RLIC), and external capsule (EC) projected onto axial slices of the John Hopkins University (JHU) atlas (z = -10).*

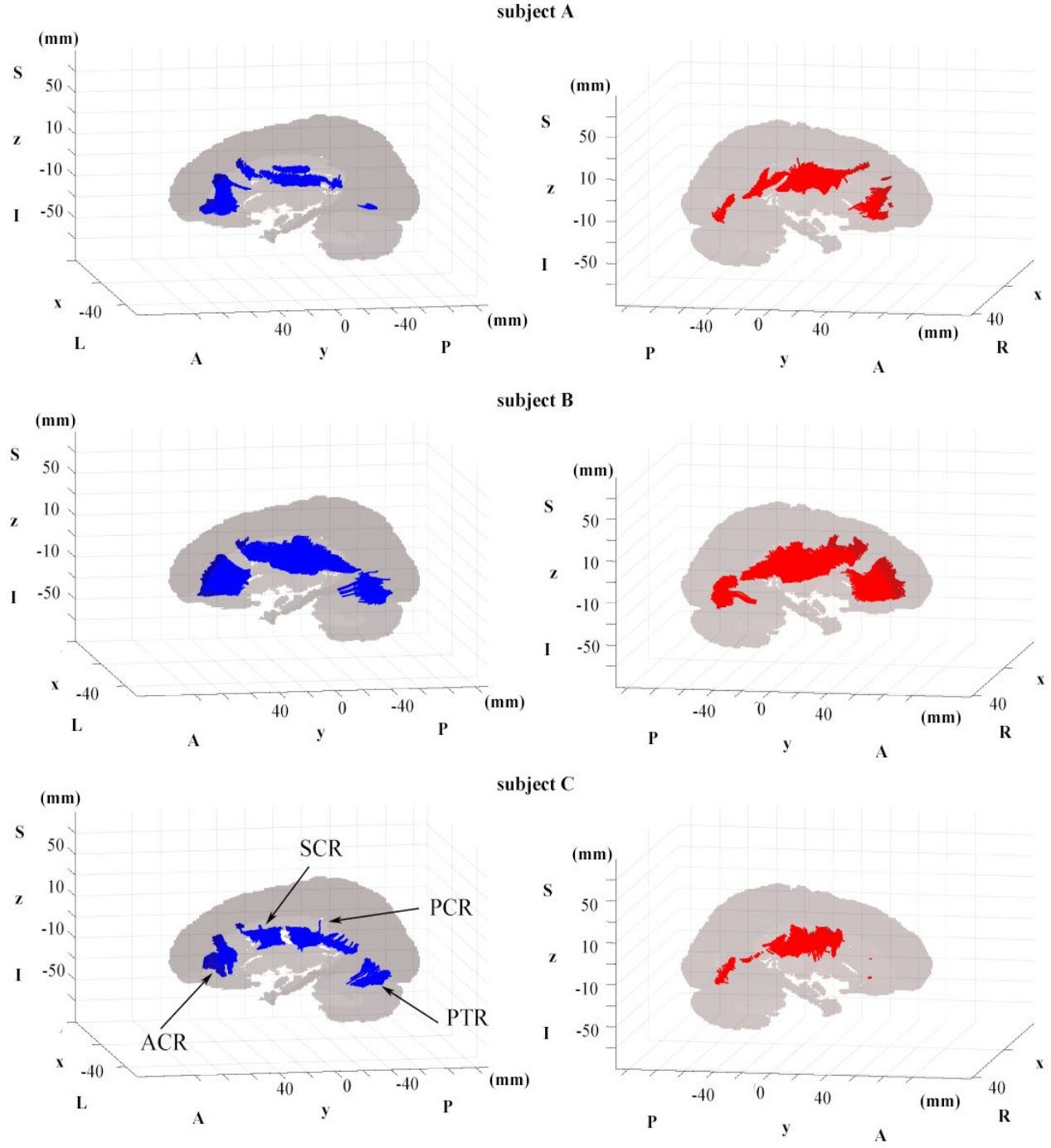

Fig. 8. *Tracked fibers in parcels posterior thalamic radiation (PTR), anterior corona radiata (ACR), superior corona radiata (SCR), and posterior corona radiata (PCR) projected onto sagittal slices of the John Hopkins University (JHU) atlas (x = 20, -20).*

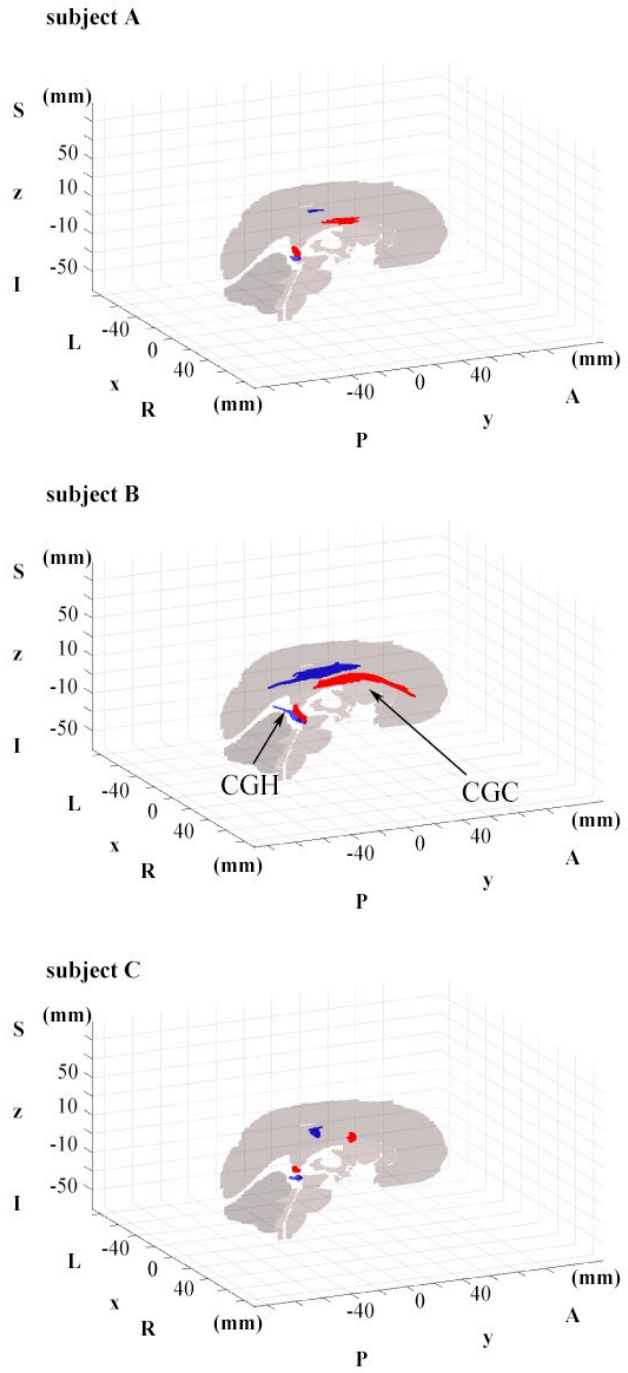

Fig. 9. *Tracked fibers in parcels Cingulum (cingulate gyrus, CGC) and cingulum (hippocampus, CGH) projected onto sagittal slices of the John Hopkins University (JHU) atlas (x = 0).*

settings usually limits number of MPG directions (and acquisition time) to reduce the load to patients. The present algorithm adopts tensor-model deterministic tracking aiming at applying to clinical dMRIs with fewer number of MPG directions. With the recent advance in MRI acquisition techniques, it is expected that HARDI (high angular resolution diffusion imaging) [25] that enables discriminating multiple fiber populations crossing within the same voxel will be applicable in the clinical settings. Future task will be to improve the fiber-tracking length, especially in the regions with crossing fibers, assuming application to HARDI data.

The proposed method aimed to obtain statistically analyzable diffusion information (such as FA and MD) automatically and comprehensively (whole-brain) based on reconstructed fiber tracts from large-scale dataset. Thus, our suggestion as a strategy may be to apply first this method to the large-scale data set to extract candidate fiber tracts of disease-specific and/or disease-common network, and subsequently examine further the extracted, limited number of candidates. At a further step of the investigation, reconstructing anatomically relevant fiber clusters by using the atlas parcels as a guide will implement local investigation based on diffusion index profiles.

CONCLUSION

We developed and proposed an automated whole-brain fiber-tracking method for dMRI combined with a white matter atlas. The validation results based on real dMRI data demonstrated the feasibility and usefulness of this method. In a future study, we plan to apply the proposed method to the dataset of patients with various neuropsychiatric disorders. Our whole-brain automated fiber-tracking method would allow a quick, objective, and easy quantitative analysis of the disruption of white matter integrity in various disorders based on large-scale multi-site dMRI data.

LIST OF ABBREVIATIONS

ACR, anterior corona radiate; ALIC, anterior limb of the internal capsule; CGC, cingulum (cingulate gyrus); CGH, cingulum (hippocampus); CP, cerebral peduncle; CST, corticospinal tracts; dMRI, diffusion magnetic resonance imaging; DTI, diffusion tensor imaging; EC, external capsule; FA, fractional anisotropy; FMRIB, functional MRI of the brain; Fx/ST, fornix (cres)/stria terminalis; IFO, inferior fronto-occipital fasciculus; MD, mean diffusivity; SCP, superior cerebellar peduncle; SCR, superior corona radiate; SFO, superior fronto-occipital fasciculus; MCP, middle cerebellar peduncle; JHU, John Hopkins University; PCR, posterior corona radiate; PLIC, posterior limb of the internal capsule; PTR, posterior thalamic radiation; RLIC, retrolenticular part of the internal capsule; ROI, region of interest; SLF, superior longitudinal fasciculus; TBSS, Tract-Based Spatial Statistics; UNC, uncinate fasciculus.

CONFLICT OF INTEREST

The authors have no conflicts of interest to declare.

ACKNOWLEDGEMENTS

This work was supported by a grant from Brain Mapping by Integrated Neurotechnologies for Disease Studies (Brain/MIND) of the Japan Agency for Medical Research and Development (AMED) and by a Grant-in-Aid for Research (15H01813) from the Ministry of Education, Culture, Sports, Science and Technology (MEXT), Japan.

REFERENCES

[1] Ashburner J, Friston KJ, Voxel-based morphometry—the methods. Neuroimage 2000; 11(6): 805–21.

[2] Smith SM, Jen-kinson M, Johansen-Berg H, et al. Tract-based spatial statistics: voxelwise analysis of multi-subject diffusion data, Neuroimage 2006;

31(4): 1487–1505.

[3] Zalesky A, Moderating registration misalignment in voxelwise comparisons of DTI data: a performance evaluation of skeleton projection. Magn Reson Imaging 2011; 29(1): 111–25.

[4] Jones DK, Cercignani M, Twenty-five pitfalls in the analysis of diffusion MRI data. NMR Biomed 2010; 23(7): 803–20.

[5] Yamamoto U, Hisada A, Kobayashi T, et al. Analyses of the disruption of white matter integrity in schizophrenia using diffu-sion tensor fiber tracking with automatic construction of region of interest. Adv Biomed Eng 2013; 2:1–10.

[6] Smith SM, Jenkinson M, Woolrich MW, et al. Advances in functional and structural MR image analysis and implementation as FSL. Neuroimage 2004; 23: S208–S219.

[7] Sherbondy A, Akers D, Mackenzie R, et al. Exploring connec-tivity of the brain's white matter with dynamic queries, IEEE Trans. Vis. Comput. Graph. 2005; 11(4): 419–29.

[8] Mori S, Wakana S, Nagae-Poetscher LM, et al. MRI atlas of human white matter. AJNR Am J Neuroradiol 2006; 27(6): 1384–85.

[9] Bracht T, Linden D, Keedwell P, A review of white matter microstructure alterations of pathways of the reward circuit in depression. J Affect Disord 2015; 187(15): 45–53.

[10] Chua TC, Wen W, Slavin MJ, et al. Diffusion tensor imaging in mild cognitive impairment and Alzheimer's disease: a review. Curr Opin Neurol 2008; 21(1): 83–92.

[11] Kubicki M, McCarley R, Westin CF, et al. A review of diffu-sion tensor imaging studies in schizophrenia. J Psychiatr Res 2007; 41(1): 15–30.

[12] Kanaan RAA, Kim JS, Kaufmann WE, et al. Diffusion tensor imaging in schizophrenia. Biol Psychiatry 2005; 58(12): 921–29.

[13] Ellison-Wright I, Bullmore E, Meta-analysis of diffusion ten-sor imaging studies in schizophrenia. Schizophr Res 2009; 108(1): 3–10.

[14] Liao Y, Huang X, Wu Q, et al. Is depression a disconnection syndrome? Meta-analysis of diffusion tensor imaging studies in patients with MDD. J Psychiatry Neurosci 2013; 38(1): 49-56.

[15] Murphy ML, Frodl T, Meta-analysis of diffusion tensor imag-ing studies shows altered fractional anisotropy occurring in dis-tinct brain areas in association with depression, Biol. Mood Anxi-ety Disord 2011; 1(3):1-12.

[16] Jenkinson M, Beckmann CF, Behrens TE, et al., FSL. Neuroimage 2012; 62(2):782-90.

[17] Faria AV, Hoon A, Stashinko E, et al. Quantitative analysis of brain pathology based on MRI and brain atlases—applications for cerebral palsy. Neuroimage 2011; 54(3): 1854–61.

[18] Faria AV, Zhang J, Oishi K, et al. Atlas-based analysis of neurodevelopment from infancy to adulthood using diffusion ten-sor imaging and applications for automated abnormality detection. Neuroimage 2010; 52(2): 415–28.

[19] Oishi K., Faria A, Jiang H, et al. Atlas-based whole brain white matter analysis using large deformation diffeomorphic met-ric mapping: application to normal elderly and Alzheimer's dis-ease participants. Neuroimage 2009; 46(2): 486–99.

[20] Mori S, Anatomy of diffusion measurement. In: Mori S, In-troduction to Diffusion Tensor Imaging, Amsterdam: Elsevier 2007; pp. 13–18.

[21] Lazar M, Weinstein DM, Tsuruda JS, et al. White matter tractography using diffusion tensor deflection. Hum Brain Mapp 2003; 18(4): 306–21.

[22] Evans DJ, A new 4th order runge-kutta method for initial value problems with error control. Int J Comput Math 1991; 39: 217–27.

[23] Parker GJM, Haroon HA, Wheeler-Kingshott CAM, A frame-work for a streamline-based probabilistic index of connectivity (PICo) using a structural interpretation of MRI diffusion meas-urements. J Magn Reson Imaging 2003 ;18(2): 242–54.

[24] Christiaens D, Reisert M, Dhollander T, et al. Global tractog-raphy of multi-shell diffusion-weighted imaging data using a mul-ti-tissue model. Neuroimage 2015; 123: 89–101.

[25] Berman I, Lanza R, Blaskey L, et al., High angular resolution diffusion imaging (HARDI) probabilistic tractography of the auditory radiation. Am J Neuroradiol 2014; 34: 1573–1578.

Received: December 26, 2017
Revised: June 20, 2018
Accepted: July 27, 2018